Charged Particle Multiplicities from Si Strip Detectors and Scintillator Tiles

H. Ito and S.J. Sanders, University of Kansas

Table Of Contents

Introduction

The number of particles emitted from a heavy-ion collision at RHIC energies provides one of the most basic characterizations of the collision process. On an event-by-event basis, this observable can be related to the centrality of the collision. By analyzing a large number of events, the observed dependence of the particle multiplicity on pseudorapidity and reaction centrality gives a measure of the "stopping" that occurs in the collisions and how the corresponding energy loss by the incident channel leads to particle production. This note discusses the charged particle multiplicity measurement obtained using the Si strip detectors and scintillator tile detectors of the BRAHMS Multiplicity Array.

At BRAHMS we have several different detector systems that measure particle multiplicities. The ZDC calorimeters measure neutron flux along the beam axis. Since all reactions of interest to our core heavy-ion program are expected to trigger both of the ZDC detectors, these devices provide an ideal minimum-bias trigger for the experiment. The ZDC "multiplicities" are, however, double valued in centrality, with both very central and very

peripheral collisions leading to the same (small) neutron multiplicities. This ambiguity prevents the ZDCs being used alone for the centrality measurement.

The first TPC (TPM1) of the mid-rapidity spectrometer measures individual tracks of charged particles and thereby provides an excellent measure of the charged particle flux into the acceptance of this detector. Further, for particles that can be tracked through the spectrometer to the time-of-flight wall, we can identify the type and charge of the particle. The mid-rapidity TPC is expected to develop the "reference" particle multiplicity distribution for the other detector systems at BRAHMS. However, the limited acceptance of TPM1 prevents its use as a multiplicity trigger. Also, TPM1 will require measurements at a number of angle settings to develop the dependence of multiplicity with pseudorapidity.

The beam-beam arrays of Cherenkov detectors provide our basic measure of the reaction vertex location. These detectors also measure charged particle multiplicities for a rapidity range closer to the beam rapidity than covered by the Multiplicity Array. Some of the preliminary data from these arrays are included in this note for comparison with the multiplicity distribution found using the Multiplicity Array.

At the time of this note, there are still many inconsistencies seen in comparing the various measurements of particle multiplicity at BRAHMS. Some, if not most, of these "problems" may be related to the different selection of events used to characterize the "centrality" of the reactions. Because of the importance of this event selection, the first part of this note discusses how the selection was done for the present analysis. Unfortunately, detailed comparison with the procedures used by other groups analyzing the mid-rapidity spectrometer and the beam-beam counter results has not yet been done. Such comparisons are seen as a "high" priority.

Overview of the BRAHMS Multiplicity Array

The Multiplicity Detector Array is used to establish overall charged particle multiplicities for collisions at BRAHMS. An inner barrel of Si strip detectors and an outer barrel of plastic scintillator "tile" detectors measure the energy loss of particles passing through the array. The detector elements are only modestly segmented so as to minimize the complexity and cost of the array. For a typical central collision, this modest segmentation results in multiple particles passing through individual detector elements. Relating the observed multi-particle energy loss to the number of particles hitting a given detector element is the principal focus of this note. A pseudorapidity range of $-2.2<\eta<2.2$ is covered for collisions occurring at the center of the array. Fig. 1 shows a picture of the Multiplicity Array away from the beam pipe.
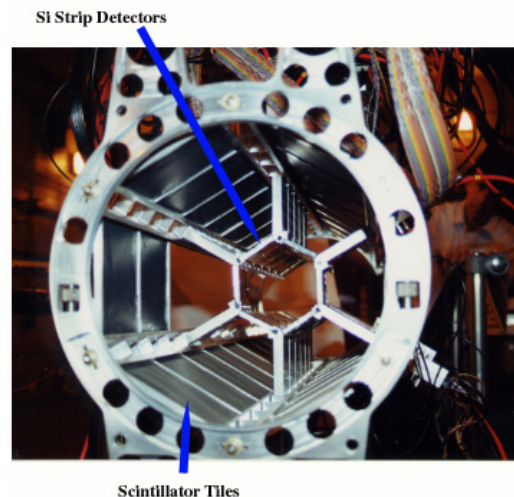

Si Strip Detectors

Scintillator Tiles

Fig. 1 - Multiplicity Array

During the year 2000 run period at RHIC, the inner barrel of Si strip detectors was comprised of 25, 4cm x 6cm x 300μm wafers, each segmented into 7 strips with a 0.86 cm pitch. The detectors were located 5.3 cm from the nominal beam axis. Both the Si strip detectors and scintillator tile detectors are arranged in six rows of detectors about the beam axis. For the Si strip detectors, three rows were populated with six wafers each, covering 42 bins in pseudorapidity, one row was populated with five wafers, and two additional rows were populated with one wafer each, allowing one "ring" about the beam axis to be fully populated. The sparse population of two sides was to accommodate a clear line-of-sight for the two-spectrometer arms and for reasons of cost.

The outer detector barrel consisted of thirty-eight, 12 cm x 12 cm x 0.5 cm scintillator tiles using a fiber-optic readout scheme were located at a distance of 13.9 cm from the nominal beam axis. Four rows were fully populated with 8 detectors, each, one row had 4 detectors, and the last row had 2 detectors. The partial population of certain rows was again done to accommodate the spectrometer arms.

Centrality Determination Using the Multiplicity Array

This section shows how the charged particle multiplicities determined by the Multiplicity Array can be used to deduce the reaction centrality. For this discussion we use particle distributions calculated using the HIJING model, where the impact parameter associated with each collision is "known", and then simulate the expected "response" of the Multiplicity Array using the GBRAHMS package.

Simulations using HIJING Model Particle Distributions

In selecting events corresponding to a given reaction "centrality" it has become common practice within the collaboration to use the sum of the energies deposited in the scintillator tiles, corrected for trivial geometric effects, as a measure of the total particle production. By this measure, we refer to the 6% of events with the greatest particle production out of all events as the 6% "most central".   In order to compare our selected events with model calculations, or even to compare our results with those of the other RHIC experiments, we need assurance that we are selecting our 6% from the pool of ALL collision events, and not a sub-pool of events having a minimum particle multiplicity threshold. GBRAHMS only records the events when there is a hit to an active detector element. However, as a measure of the efficiency for detecting events, we can compare the number of input events to the simulation with the number leading to tile "hits".   The result of this study, using a HIZING calculation that covers impact parameters from 0 fm to 20 fm, indicates close to 100% probability of at least one measurable particle hitting a scintillator tile element in the array. For this study, a "measurable" particle was defined as one with an energy loss in a tile element that is at least six times the standard deviation of the pedestal width. With this criteria, only 0.1% of the model events are "missed" by the array.   Fig. 2 shows the impact parameter distribution for HIJING model. In this figure, three different centrality cuts, based on impact parameter, are shown in different colors.

Since the impact parameter is not measured experimentally, a different observable is necessary to characterize the reaction centrality. For BRAHMS, the charged particle multiplicity found using Si and tile detectors is used. The details of the multiplicity determination are discussed later. Based on the simulations, Figures 3 and 4 compare multiplicity based centrality cut with the actual centrality based on impact parameter.
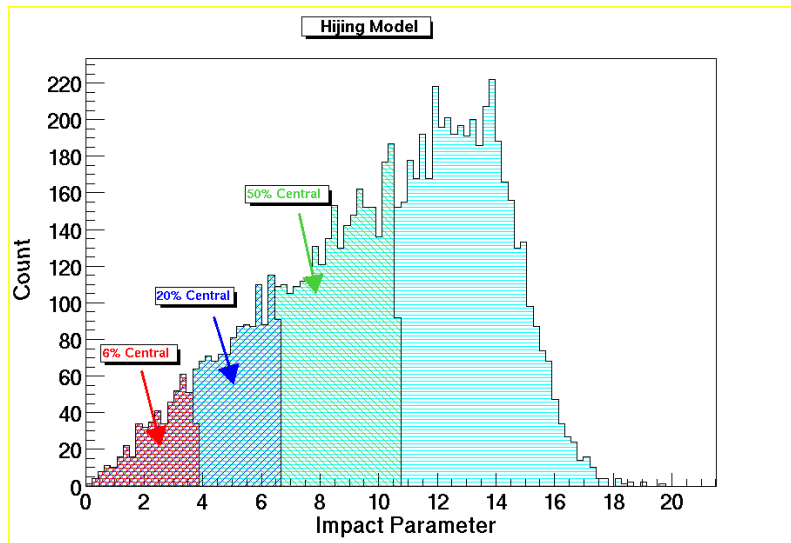

Figure 2: Impact Parameter Distribution of HIJING Model

Looking at these figures, one sees that the multiplicity-based centrality selects a wider distribution of impact parameters than one would obtain with a direct, but experimentally unachievable, cut on the impact parameter. However, the average impact parameter for each of the centrality cuts in Figure 4 is fairly close to that of Figure 2.
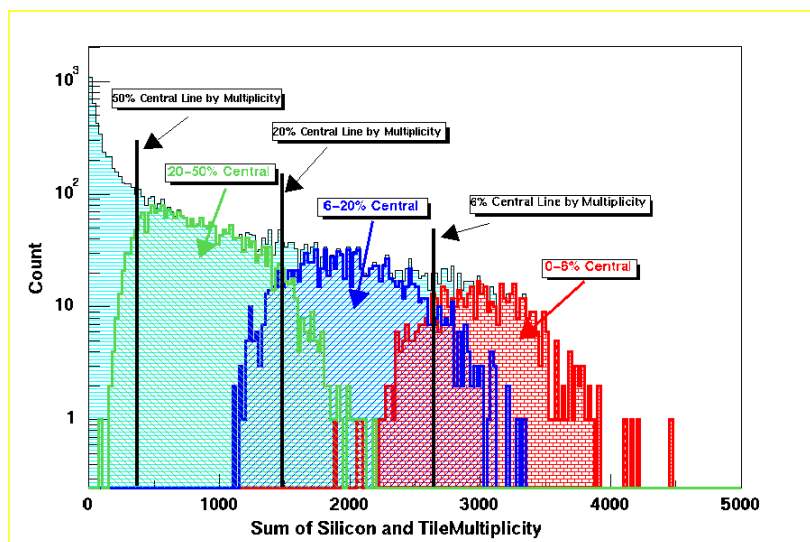

Figure 3: Distribution of Sum of the Silicon and Tile Multiplicity based on GBRAHMS simulation using HIJING input events.
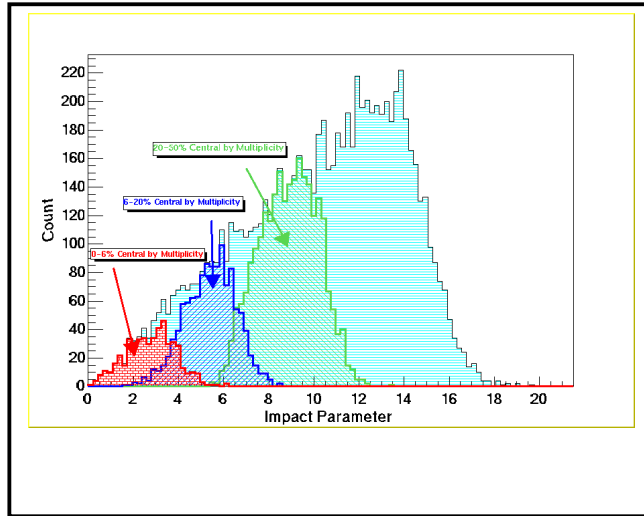
4

Figure4: Impact Parameter Distribution with Multiplicity-based Centrality Cut

Experiment

In the analysis of the experimental data, the same multiplicity based centrality is going to be used. However, there is an additional complication of needing to select only those events that correspond to Au+Au collisions, and not include events corresponding to beam-gas interactions. For this analysis, run 2336 is used with a very narrow vertex cut around z=0 cm. A correction is applied for the (small) vertex dependence of the deduced multiplicity.

The easiest way to look at the background events is to plot ZDC sum-ADC against the multiplicity measured in one of the other global detectors. Figure 5 shows this comparison using the BB array multiplicity with the condition that the tiles have at least one hit. In this figure, the area enclosed by the red line locates the background events.

The background events can be largely eliminated by selecting only those events where the BB and the ZDC vertices are within 15 cm from each other, or
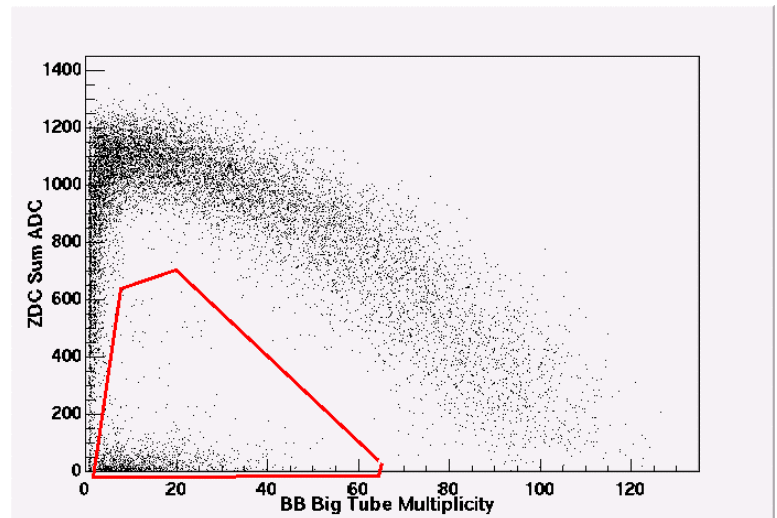

Figure 5

events for which only the ZDC decides the vertex because no corresponding BB vertex can be established. This is shown in Fig. 6 where one sees a relatively few counts in the "background" region. However, Fig. 7 shows the sum of Si and tile multiplicities using this event selection. By comparing Fig. 7 and Fig. 3, the HIZING based distribution, there still seem to be far too many low multiplicity events.
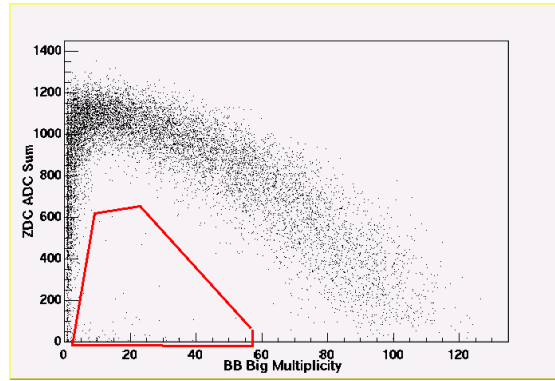
Figure 8 shows two correlation plots based on tile and Si multiplicities. The left figure plots the sum of these multiplicities, corrected for the different geometric efficiencies of the two arrays, as a function of the difference of the two multiplicities. (Throughout this report, the Si raw multiplicity has been scaled by a factor of 1.468 to obtain a consistent measure with the tile array. This factor is the ratio of geometric acceptances of the two arrays.) The regions indicated by the red lines correspond to spurious events. The red area to the right (left) corresponds to events that have high silicon (tile) multiplicity with low tile (silicon) multiplicity. The right figure shows a plot of the difference in the two multiplicities divided by their sum. Again, the red area indicates the existence of uncorrelated events. Figure 9 shows the same plot by the GBRAHMS simulation, with the axes switched for the 2-D histogram. The excess in events where too high a Si multiplicity is recorded is largely a consequence of the poor resolution of singe-hit events in these detectors.
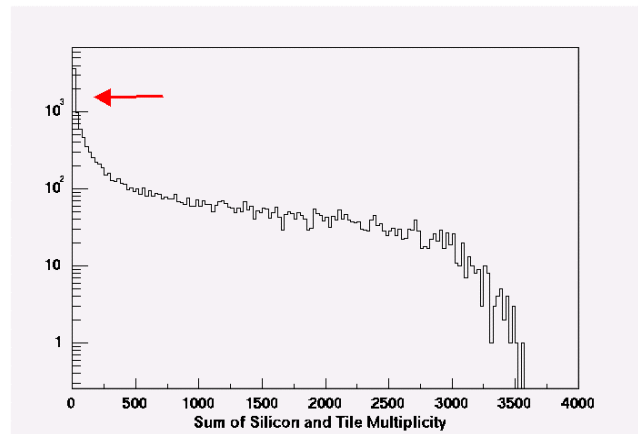

Figure 6: ZDC ADC Sum vs. BB Big Tube Multiplicity

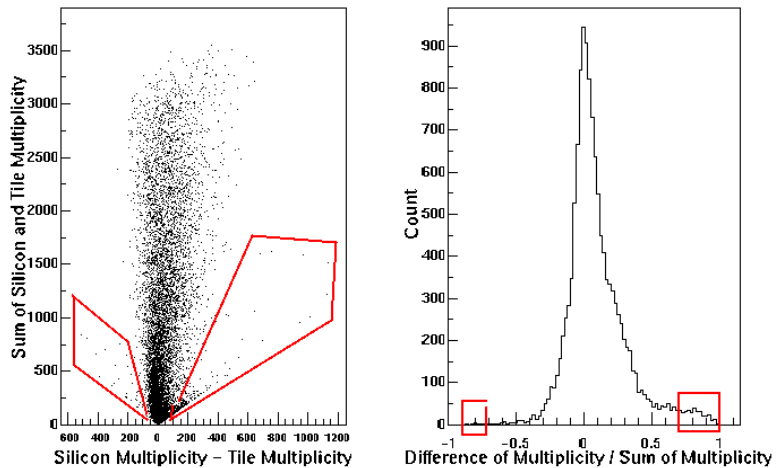*Figure 7: Experimental Sum of Multiplicity Distribution.*

Figure 8: Correlation plots of Silicon and Tile Multiplicity

6

To reduce the spurious events seen in the data, the following cut is applied:

$$\left| \frac{multSi - multTiles}{multSi + multTiles + 10} \right| < 0.7$$

Although by using this selection some real events (less than 1% based on the data shown in Figure 9) are lost, most of uncorrelated events between the silicon and tile arrays are eliminated. With this cut, the correlation between the two multiplicities is again shown in Fig. 10 and the sum of multiplicity distributions is shown in Figure 11. By comparison with Figure 3, the low-multiplicity behavior now looks more reasonable.

Finally, using the data in Figure 11, Figure 12 shows the centrality cuts used for analysis.
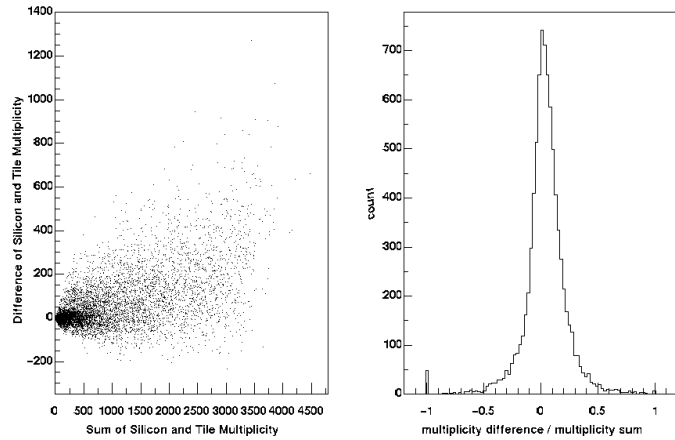
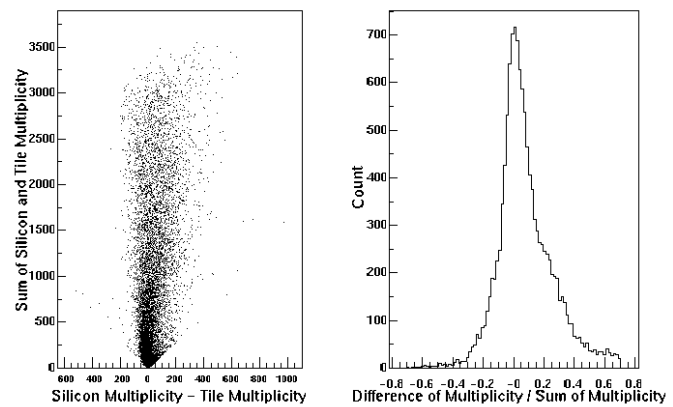

Figure9: Similar to Figure 7 but based on HIJING model

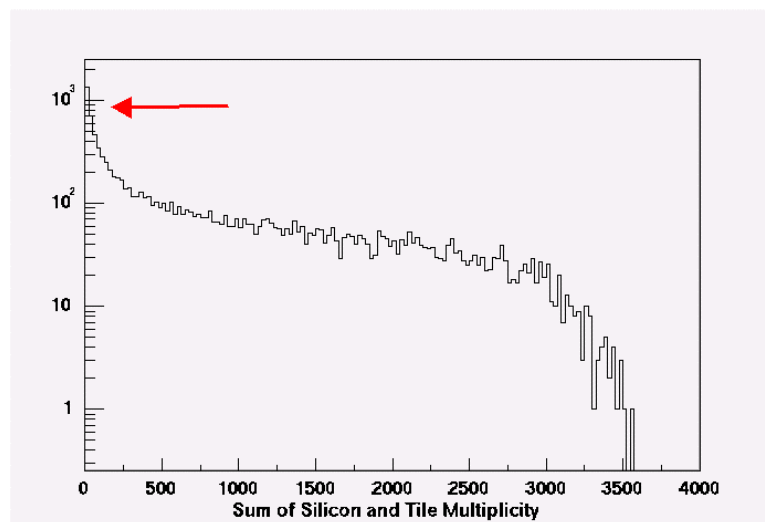
Figure 10: Same as Fig. 8, but with cut discussed in text.

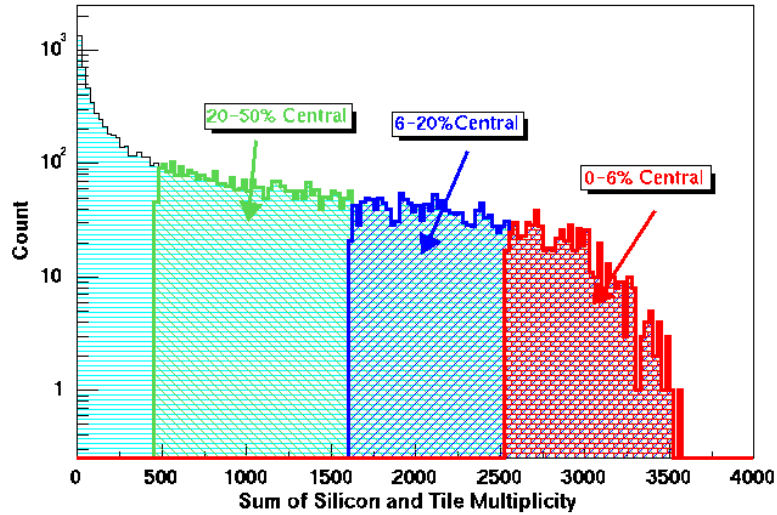Figure 11: Sum of experimental multiplicity distributions for
the Si and Tile arrays.

7

Figure12: Centrality cuts used for the analysis
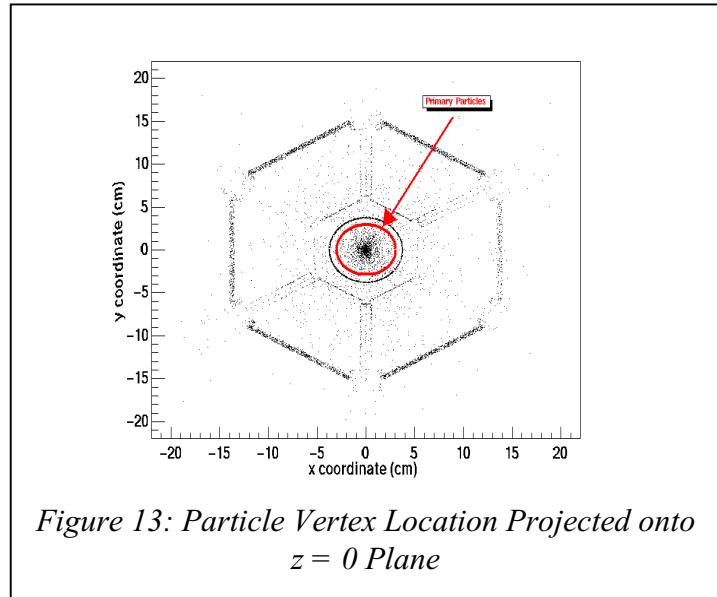
Charged-Particle Multiplicities (dN/dη)

This section develops the procedures used to extract charged particle multiplicities from the experimental data.

Method

Definition of "Primary" particles

First, the definition of "primary" particle needs to be discussed. There are several ways to define this term. The most obvious is to take all particles coming from the original collision vertex that strike the detector as "primary". Although this seems reasonable, the definition excludes all short-lived particles and, consequently, is model dependent. Some models (such as Fritiauf) give a particle distribution that already accounts for short-lived particle decays. Other models (such as HIJING) quote a particle distribution from an earlier stage of the reaction. Although the difference is small (on the order of several percent), it needs to be considered. Another possible definition of "primary particle" is to take those particles coming from the original vertex which would have hit a detector if there are no decays for secondary scattering effects as primary. This definition suffers by including particles that do not actually hit any detectors. For this note, we define as "primary" those particles that originate in a small sphere around the original vertex. This is an improved version of the first definition. It includes the daughter products of short-lived particles, thereby reducing the model sensitivity. This definition also comes closest to what can be experimentally verified by using the TPM1 results. Figure 12 shows the plot of particle vertex location projected onto z = 0 plane using

8

GBRHAMS with HIJING model events. The area enclosed by the red line indicates the vertices of the primary particles. The other particles are defined to be secondary particles.

Figure 13: Particle Vertex Location Projected onto z = 0 Plane

Number of Primary Particles in a Strip or Tile.

The procedure used to extract particle multiplicities from the data is shown schematically in Figure 14. First, an ADC value is transformed into the corresponding energy value, as represented by the function calls SiE (ADC, ch) and TileE(ADC,ch). (The details of the energy calibration will be forthcoming. An earlier discussion can be found at http://www.phsx.ukans.edu/~sanders/MultiplicityAnalysis.) Then, using transformation functions derived from GEANT simulations, the energies are converted on an event-by-event basis into the number of primary particles, here represented by the function calls SiN (E,eta) and TileN(E, eta, column number of tile).
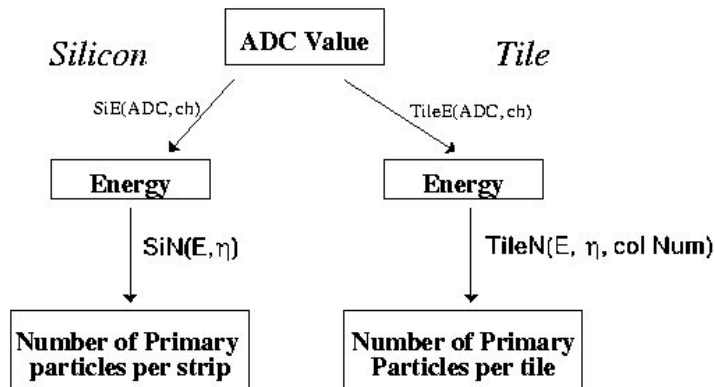

Figure 14: General Diagram for Calculating Number of Primary Particles

To obtain the conversion functions (SiN and TileN) from the detected energy to the number of primary particles, we use the following method. From the GEANT simulation, the mean number of primary particles for each strip or tiles is first obtained, using a 6% centrality cut. Typical distributions are shown in Figure 15. For each Si strip, the number distribution of primary particles follows Poisson-like statistics. For the tile detectors, the distribution is close to Gaussian. In either case, the mean value is well established.

Next, the mean value of the detected energy is determined for each silicon strip and scintillator tile based on the same simulation. This includes not only the energy loss of the primary particles but also the energy deposited by the secondary particles. The goal is to obtain an inclusive conversion function from observed energy to number of primary particles. The
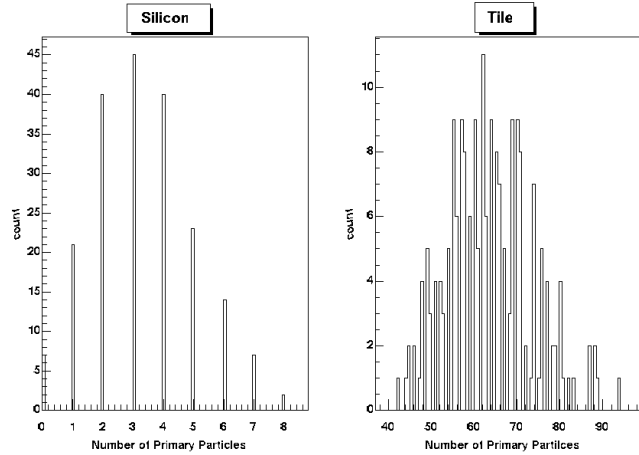

Figure 15: Typical Primary Particle Distribution for Silicon and Tile

dependence of the detected energy on the particle track length inside the active detector volume as well as background contributions are included. This conversion function does have some model dependence. In particular, the stopping power of particles passing through the detector elements (dE/dx) is not quite constant because of its dependence on the particle momentum as well as the mixture of particle type. This can be easily understood by considering the Bethe-Block formula. Figure 16 and 17 show the dE/dx plots for pions in the silicon and the tiles within the applicable momentum range. Within the array, the peak value of the momentum of pions is expected to be in the range of 0.3-0.5 GeV/c, depending on angle, with the distributions dropping to 10% of their peak values for momenta in the range of 1-2 GeV/c, depending on angle, and also falling off steeply for momenta below about 0.2 GeV/c. As seen, within this range, the stopping powers are not constant, but rather deviate 5 % or more.
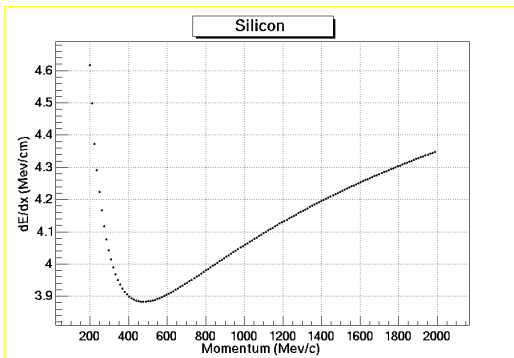

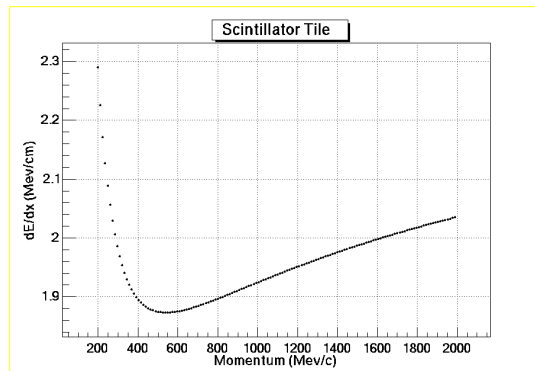*Figure 16: dE/dx for Pion in Silicon Strip Detector*

Figure 17: dE/dx for pions in scintillator tiles.

The range of stopping powers becomes even greater for heavier particles, as shown in Fig. 18 for kaons in the silicon strip detectors. The peak of the kaon momentum distribution varies from 0.4-1.2 GeV/c for the angular range covered by the multiplicity array. Fortunately, the particle distribution is dominated by pions and the momentum and particle mix does not appear to be strongly model dependent.
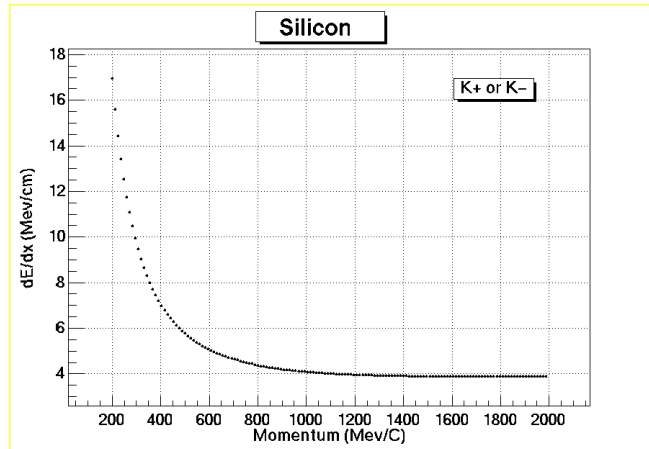

Figure 18: dE/dx for Kaon in Silicon Strip Detectors

Since the silicon strip and the scintillator tile are relatively thin, the detected energies follow a near-Landau distribution with very asymmetric shapes. To obtain a mean energy, for now these distributions are being fitted with Gamma distributions that appears to well reproduce the simulated distributions. This is done rather than simply taking the mean value of the "observed" distribution because of the very limited statistics of the GBRAHMS simulations and the consequent fluctuations observed when taking the means. The fits introduce a potential systematic error that we should be able to reduce by generating some very long GEANT runs.

After obtaining the mean number of the primary particles and corresponding mean energy for a given Si strip and tile, the ratio is taken as the energy-to-hits conversion factor. By repeating this process for many different vertices in GBRAHMS, conversion functions are developed for a range of pseudorapidities. Figure 19 and 20 show these functions for the Si and tile detectors, respectively. A single function is found to do a good job in characterizing all of the Si strips, while 8 functions, corresponding to each tile ring around the beam pipe, are needed to describe the scintillator tile detectors. The reason for this is that the detected energy in the tiles has a large contribution from the secondary particles (30-45%), and this secondary rate is highly sensitive to the configuration of the detectors. Since the detected energy contribution of the secondary particle in the silicon detectors is smaller (6 - 20%), the ring-by-ring correction does not appear to be necessary.
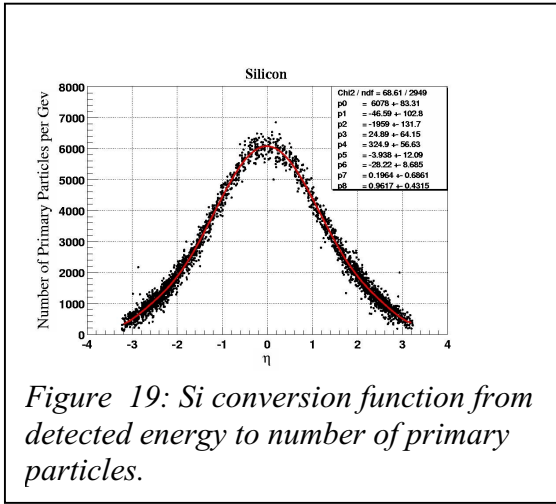
Figure 19: Si conversion function from detected energy to number of primary particles.
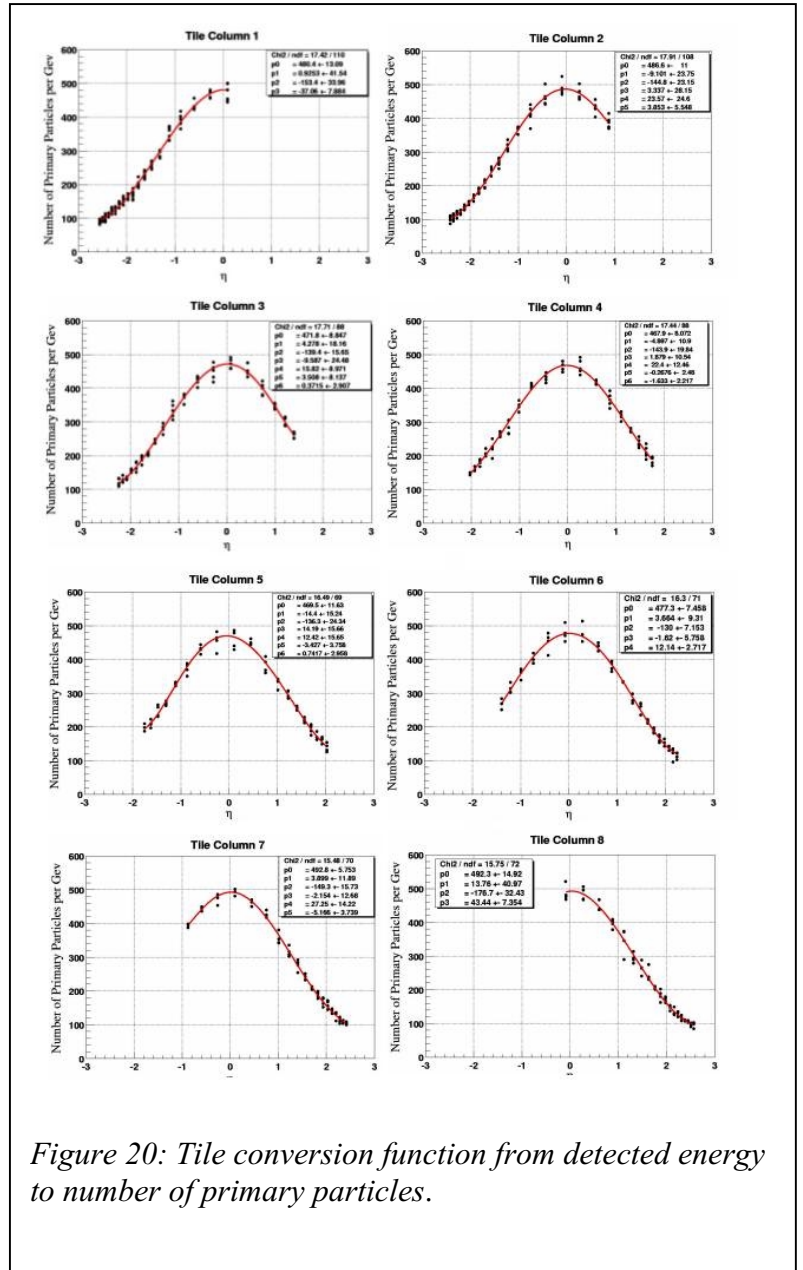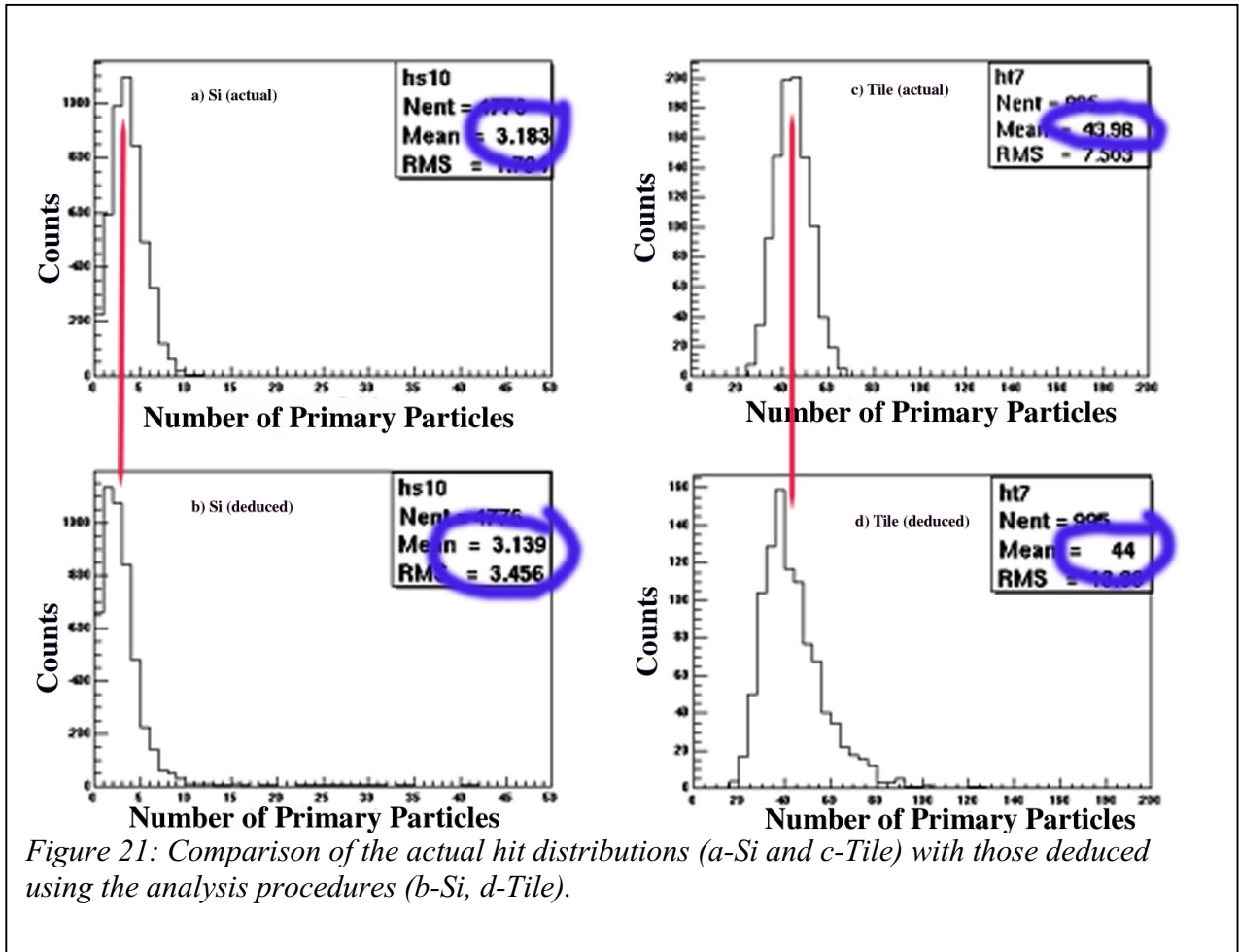

Figure 20: Tile conversion function from detected energy to number of primary particles.

12

It is necessary to be somewhat careful in working with the "primary hit" distributions that are obtained using the procedure described above. This procedure results in hit distributions that reflect the truncated-Landau tails of the original energy distributions, as seen in Fig. 21. Figures 21a and 21c show the actual hit distributions for typical Si and Tile detectors, respectively. Figures 21b and 21d show the corresponding distributions recovered using the above procedures. Although there is a clear shift in the peak locations of the actual and recovered distributions, the mean values of the distributions (as circled in the figure) are found to be very close.

Figure 21: Comparison of the actual hit distributions (a-Si and c-Tile) with those deduced using the analysis procedures (b-Si, d-Tile).

Although the importance of the distribution tails in determining the mean value of the deduced hit distributions is not that obvious with the limited statistics GBRAHMS simulation, Fig. 22 shows representative distributions obtained from the experimental data for the Si and tile detectors. Here the influence of the Landau-like tail is clear for the Si element. The thicker tile elements are not as strongly influenced by this effect.
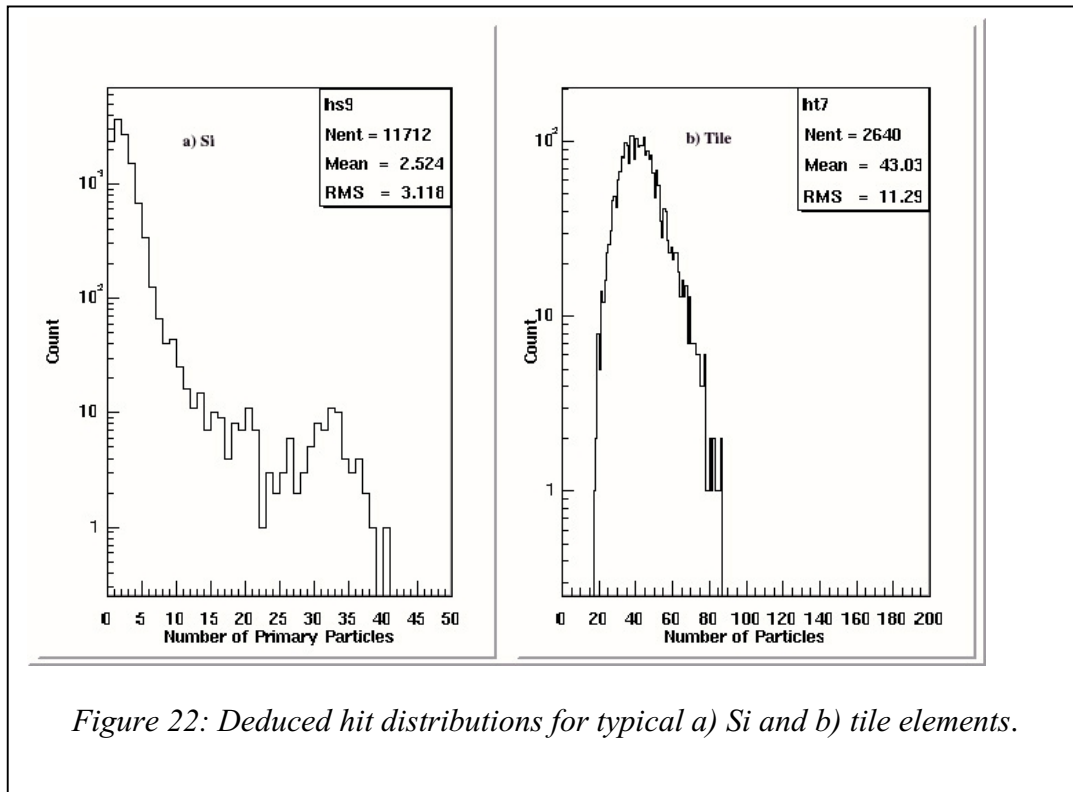
Figure 22: Deduced hit distributions for typical a) Si and b) tile elements.

Δη

Conversion of the number of particles hitting a detector element to a corresponding value of dN/dη requires finding the geometric acceptance of the detector. Because an extended range of vertex locations is used in the analysis, for any given detector element the effective solid angle may vary significantly. In the present analysis, the solid angles for each element is calculated on an event-by-event bases, using the vertex location determined by the BB array or, if the BB vertex is not developed, using the ZDC determined vertex. Figure 23 illustrates how Δη is defined for a finite thickness detector.

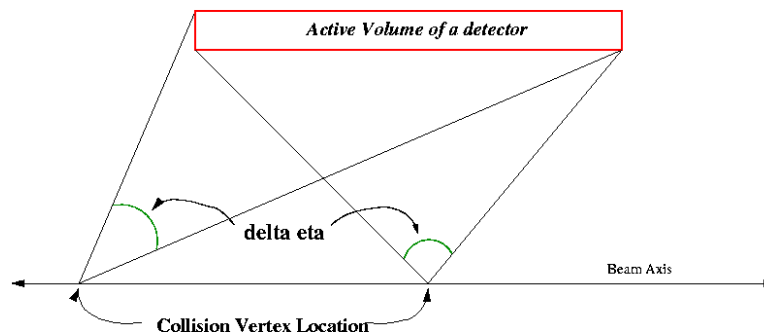*Figure23: Definition of Δη*

14

dN/dη

   Once the average number of primary particles and the corresponding Δη values are determined, it is possible to obtain a corresponding dN/dη values.

Checking the method.

   The procedures outlined above can be checked using simulated events.   A pseudo event file was first created using HIJING central events and GBRAHMS. Comparisons of "known" dN/dη distributions (filled circles) with those obtained using the analysis steps outlined above (stars) are shown in Figure 24 and 24 at vertex locations of z = 0 and z = +10 cm, respectively. The lines indicate the HIJING model input that went into the GBRAHMS simulation. As seen, the method of determining the dN/dη works quite well for both silicon and tile detectors. The difference in the input distributions as represented by the lines with the "expected" values results from the definition of "primary" particles employed in our analysis.
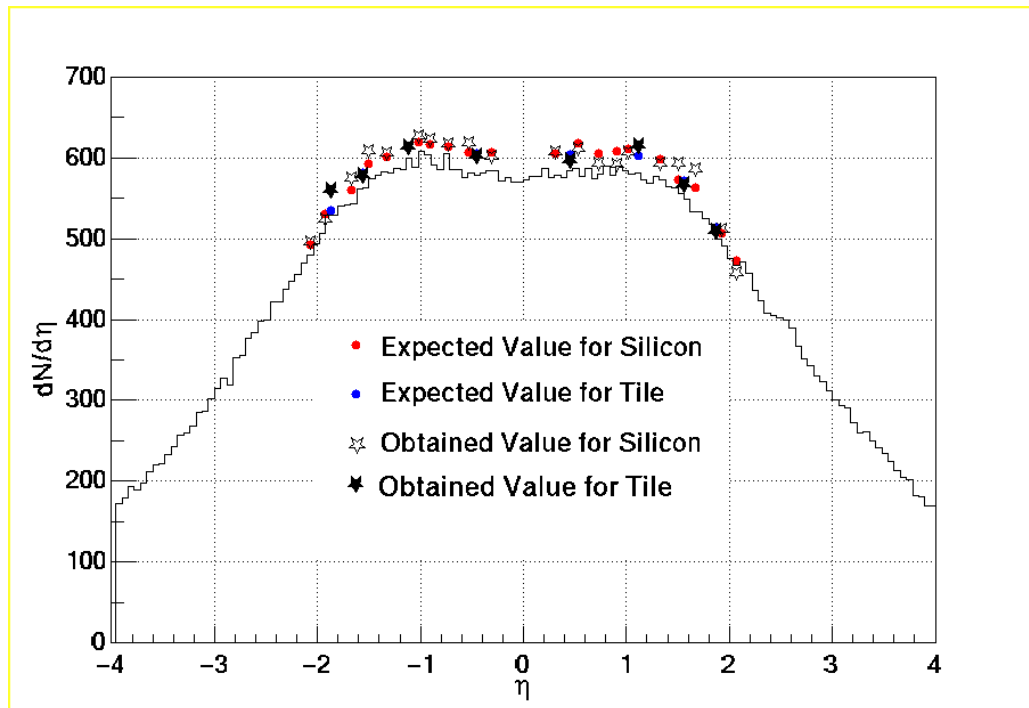

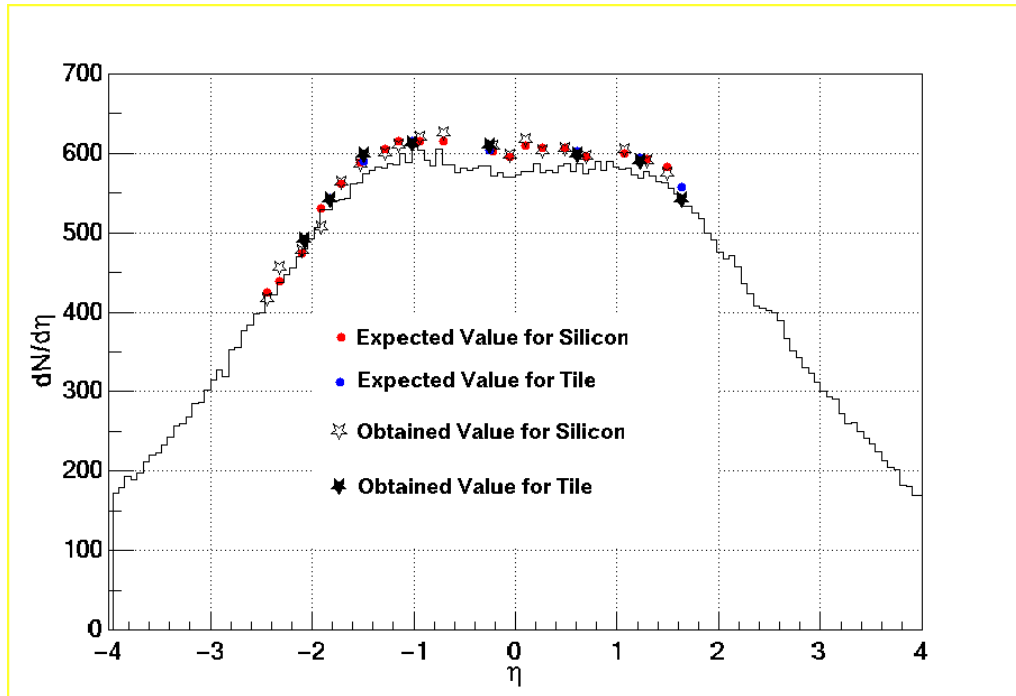*Figure 24: Expected and Obtained dN/deta at Vertex at z = 0 cm*

15

Figure 25: Same as Figure 24 with Vertex at z = +10 cm

Comparison of Calculations to Experimental Results

HIJING model

The HIJING model with a 0-20 fm impact parameter range was used to obtain model prediction for the dN/dη distributions. Using centrality cuts based on impact parameter and as shown in Fig. 2 leads to the model predictions that are shown in Fig. 26 for three different centrality cuts.
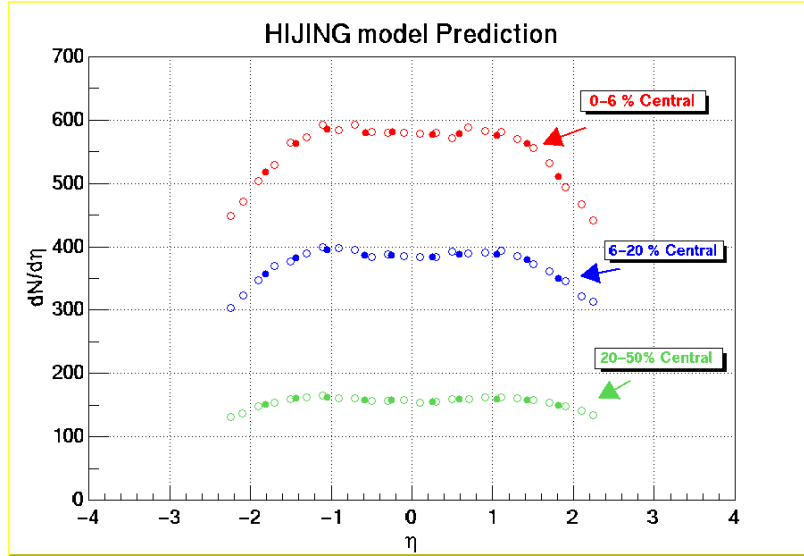
Figure 26: HIJING Model Prediction. Open and Solid Circles are for Silicon and Tile respectively

Experimental Data

Figure 27 shows the experimental dN/dη distributions obtained from run 2336. The centrality cuts are shown in Figure 11 for three different centrality selections. Also shown in this figure are preliminary dN/dη results from the beam-beam detector arrays for the most central events (see the analysis note by Y. Blyakhman.) The HIJING model prediction, before correcting for short-lived particle decays, are also shown. Adjusting for these decays would raise the HIZING predictions in the mid-rapidity region, as seen in Figures 24 and 25.

For the central events, the distribution is very symmetric for both the silicon and the tile detectors. Also, the BB detector matches well with the silicon and tile results. However, for more peripheral events, the distribution by the silicon detectors is not symmetric whereas that of tiles is still quite symmetric. This suggests that a multiplicity dependence of vertex location may still exist in the BB calibrations.
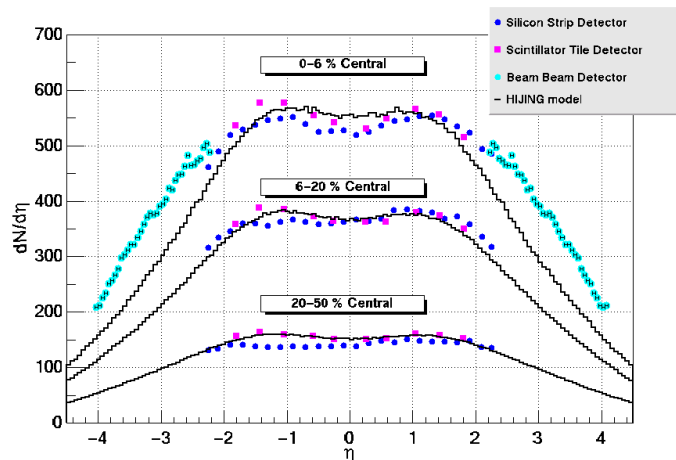

Figure 27: Experimental dN/dη distributions. The lines show the corresponding HIJING predictions before correction for short-lived particles.

The experimental dN/dη distributions have been rescaled by the number of participants by first using the HIZING model simulations to relate the centrality cuts to cuts on impact parameter, and then using Glauber model calculations to determine the average number of participants for the corresponding impact parameter range. The number of participants assumed for the different centrality cuts used in this report are tabulated below:

cut	number of participants
0-6	334
6-20	239
20-50	106
0-5	338
5-10	289
10-15	239
15-20	201
20-25	168
25-30	139
30-35	114
35-40	92

Using these values for the number of participants, the dN/dη distributions per participant pair for the Si and tile detectors is shown in Figure 28.   It is clear that with this scaling, the differences observed for the Si and tile detectors gets greatly accentuated for the more peripheral reaction cuts.

In Fig. 29, the results of the experimental dN/dη per participant pair results for mid-rapidity (η=0) events are shown as a function of the number of participants. The BRAHMS results are based on the Si data. Also shown are the preliminary results quoted by the PHOBOS and PHENIX groups at Quark Matter 2001 and the value obtained from pp scattering data.
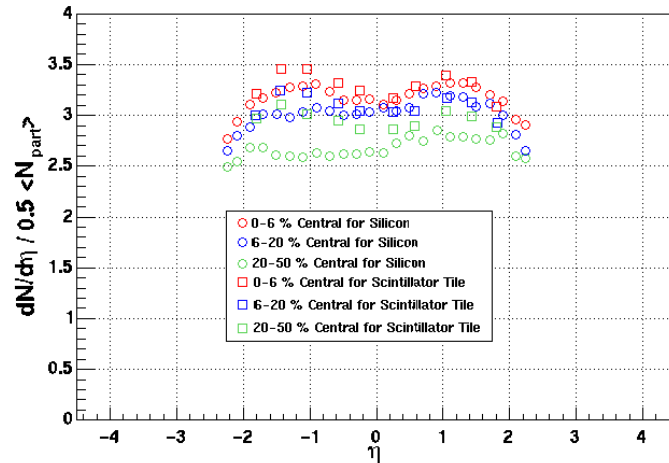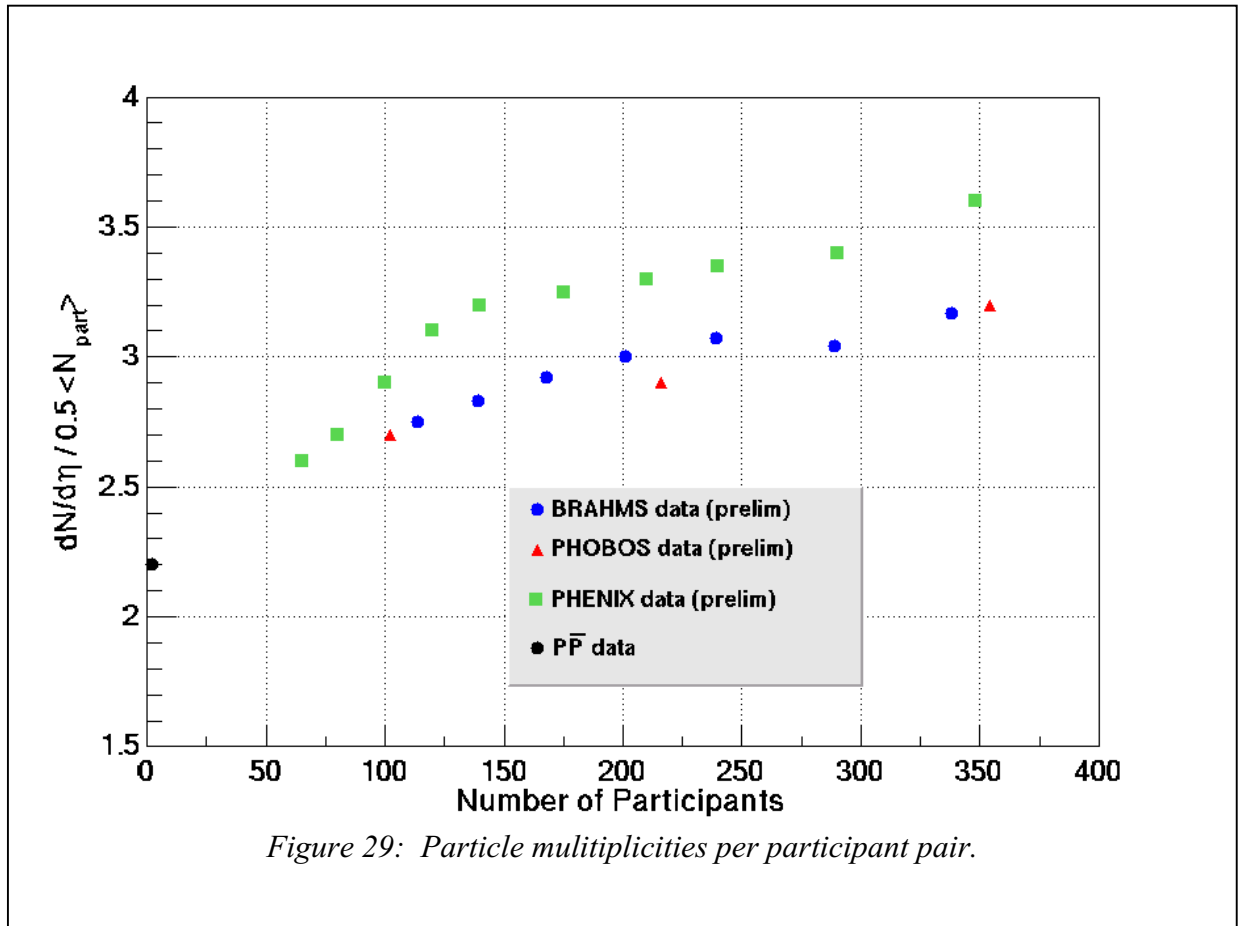

Figure 28: Experiment dN/dη distributions per participant pair.

18

Figure 29: Particle mulitiplicities per participant pair.

Uncertainty Analysis

The heading is just a teaser. This is a non-trivial analysis that has hardly begun. The major elements that we know will contribute include:

- Energy calibration of Si and Tiles. This will primarily enter as a systematic shift of all of our results. We believe that the current calibration is good to about 7%, and hope that this uncertainty can be reduced further.
- Conversion factors from energy to number of particles. Since these correction factors depend on the vertex location, the systematic errors that they introduce may be dependent on pseudorapidity.

All other uncertainties, statistical and otherwise, are believed to be small compared to these two. Our best guess as to our overall systematic uncertainty is 10%. Quoting 15% would be very conservative.